Boundary-Layer Meteorol (2015) 155:87–109
DOI 10.1007/s10546-014-9991-6

ARTICLE

Enhancing Hydrologic Modelling in the Coupled Weather Research and Forecasting–Urban Modelling System

Jiachuan Yang · Zhi-Hua Wang · Fei Chen · Shiguang Miao · Mukul Tewari · James A. Voogt · Soe Myint

Received: 1 June 2014 / Accepted: 2 December 2014 / Published online: 23 December 2014

Abstract Urbanization modifies surface energy and water budgets, and has significant impacts on local and regional hydroclimate. In recent decades, a number of urban canopy models have been developed and implemented into the Weather Research and Forecasting (WRF) model to capture urban land-surface processes. Most of these models are inadequate due to the lack of realistic representation of urban hydrological processes. Here, we implement physically-based parametrizations of urban hydrological processes into the single layer urban canopy model in the WRF model. The new single-layer urban canopy model features the integration of, (1) anthropogenic latent heat, (2) urban irrigation, (3) evaporation from paved surfaces, and (4) the urban oasis effect. The new WRF–urban modelling system is evaluated against field measurements for four different cities; results show that the model performance is substantially improved as compared to the current schemes, especially for latent heat flux. In particular, to evaluate the performance of green roofs as an urban heat island mitigation strategy, we integrate in the urban canopy model a multilayer green roof system, enabled by the physical urban hydrological schemes. Simulations show that green roofs are capable of reducing surface temperature and sensible heat flux as well as enhancing building energy efficiency.

J. Yang · Z.-H. Wang (✉)
School of Sustainable Engineering and the Built Environment, Arizona State University, Tempe, AZ 85287, USA
e-mail: zhwang@asu.edu

F. Chen · M. Tewari
National Center for Atmospheric Research, Boulder, CO 80307, USA

S. Miao
Institute of Urban Meteorology, China Meteorological Administration, Beijing 100089, China

J. A. Voogt
Department of Geography, University of Western Ontario, London, ON N6A 5C2, Canada

S. Myint
School of Geographical Sciences and Urban Planning, Arizona State University, Tempe, AZ 85287, USA

Keywords Green roofs · Hydrological modelling · Regional hydroclimate · Urban canopy model · Urban irrigation · WRF model

1 Introduction

Global population has become increasingly urbanized: to date 52 % of the world's population live in cities, and this proportion is projected to increase to 67 % by 2050 (United Nations 2012). Natural terrains are continuously converted to urban landscapes to meet the ever-increasing demand of the expanding urban population. Urbanization changes the surface energy and moisture balance, leading to significant modification in local and regional hydroclimate (Zhang et al. 2009; Song and Wang 2014). On the other hand, global climate change is forecast to cause more frequent occurrences of climatic extremes, such as heat waves and severe floods, imposing additional challenges on urban environment (Field et al. 2014). The combination of rapid urban growth and climate change places stringent constraints on energy and water sustainability, and makes cities more vulnerable to a number of environmental problems (Arnfield 2003).

It is therefore imperative to understand the combined effects of future urbanization and climate change to develop adaptation/mitigation strategies for the anthropogenically-induced environmental problems. During the past decade, numerous urban canopy models have been introduced into mesoscale models to represent land-surface processes and provide realistic lower boundary conditions for the overlying atmosphere (e.g. Martilli et al. 2002; Chen et al. 2004). To model the exchanges between the land surface and the atmosphere, mesoscale atmospheric and urban canopy models are coupled, whereby mesoscale models predict meteorological forcings for the surface. Among coupled frameworks, the Weather and Research Forecasting (WRF)–urban modelling system has been widely applied to numerical weather predictions, regional climates, emergency responses, air quality, and water resources. Chen et al. (2011) evaluated the skill of the coupled WRF–urban modelling system for assessing urban environmental problems and its cross-scale modelling capability. Currently four urban parametrization options are available in the WRF model that are coupled to the Noah land-surface model, namely the bulk parametrization, the single-layer urban canopy model (SLUCM) (Masson 2000; Kusaka et al. 2001), the multi-layer urban canopy model (Building Energy Prediction, BEP) (Martilli et al. 2002), and the BEP model plus indoor-outdoor exchange building energy model (Salamanca et al. 2010). The coupled WRF–urban modelling system has been applied to major metropolitan regions and its performance has been validated against a wide variety of ground-based observations, including atmospheric soundings and wind-profiler measurements. Mid- to end-of-century urban climates have also been studied with the modelling system (Kusaka et al. 2012b). Meanwhile, other studies have examined the impacts of different urban parametrizations on model simulations of energy balance components, near-surface air temperature, the wind field and the atmospheric boundary-layer height (Kusaka et al. 2001; Salamanca et al. 2011; Song and Wang 2014). Overall, the model performance of the Noah/SLUCM system is robust and captures realistically urban land-surface processes.

In coupled mesoscale atmosphere-urban modelling systems, the accuracy of atmospheric model fields depends on the parametrization of urban landscapes (Song and Wang 2014). An international effort was conducted to compare a wide range of these urban parametrization schemes and to evaluate them against site observations (Grimmond et al. 2010, 2011). This comparison identified the latent heat flux as that quantity for which the models demonstrate the least capability. This is because most models are inadequate in calculating the

urban water budget due to the oversimplified representation of complex urban hydrological processes and urban vegetation. Various problems exist: for example, Masson (2000) modelled surface intercepted water as small reservoirs and took snow effects into consideration in urban areas, but without resolving the anthropogenic water budget explicitly. Lee and Park (2008) and Wang (2014a) included tall trees in the SLUCM but neglected sub-surface moisture transport. In the current Noah/SLUCM system, Kusaka et al. (2001) use a tile approach to represent urban vegetation, where total fluxes are estimated as the areal average of fluxes from impervious and vegetated surfaces. Other than urban vegetation, the only hydrological process considered is evaporation after rainfall events; the evaporation is simulated using a hypothesized saturated surface with an evaporation parameter. And there are urban canopy models that simply do not consider vegetation and calculate no latent heat flux, even after rainfall (Grimmond et al. 2010). The net effect of these simplified representations of urban hydrological processes is that the root-mean-square error between the predicted and observed latent heat fluxes can be as large as the latent heat flux itself (Grimmond et al. 2010, 2011). This consequently introduces significant errors into the atmospheric hydrological cycle via land–atmosphere interactions.

An accurate representation of the water budget is therefore critical to understanding the hydrological processes in urban areas. Compared to natural landscapes, urban environments consist of a considerable fraction of paved surfaces. Though a pavement is able to store water due to surface porosity, local slope gradient and surface depressions, evaporation from paved surfaces has been largely neglected in urban canopy models. Evaporation arising from water-holding pavement surfaces, especially during and shortly after precipitation, contributes a substantial fraction of moisture fluxes arising from a built environment (Ramamurthy and Bou-Zeid 2014). Another dimension of complexity in urban hydrology arises from the anthropogenic sources, examples including water release from commercial buildings and urban irrigation. In addition, and in contrast to natural terrain, a considerable fraction of urban vegetation presents as isolated patches, such as hedges, roadside trees, and garden plants. Along the upwind edge of a vegetation canopy surrounded by a lower roughness surface, due to the lack of obstacles to the receipt of radiation and to the airflow, the advection and 'clothesline effect' (Hagishima et al. 2007) lead to higher rates of evapotranspiration. Patchy urban vegetation has therefore higher rates of potential evapotranspiration, a phenomenon known as the oasis effect (Oke 1979).

To address the challenges in modelling the urban water cycle, Wang et al. (2011a, 2013) developed an improved SLUCM to incorporate detailed hydrological processes, including evaporation from vegetated and engineered surfaces, sub-facet heterogeneity for water transport, and multilayer green roof systems. The capability of the model has been validated using field measurements under different climate conditions (Sun et al. 2013; Wang et al. 2013). More recently, Miao and Chen (2014) introduced urban irrigation, the oasis effect, and anthropogenic latent heat into the Noah/SLUCM system. Inspired by this recent work, the aim of the present study is to further improve and test the reliability and predictability of the integrated Noah/SLUCM modelling system incorporating physically-based representation of urban hydrological processes. Our objectives are: (1) to enhance and evaluate the modelling of urban hydrological processes in the current Noah/SLUCM system, and (2) to assess the capacity of physical parametrizations of multilayer green roofs in mitigating urban environmental problems at the city scale. Numerical simulations are driven by meteorological forcing and compared against the surface energy budget, both obtained from eddy-covariance measurements at four metropolitan sites, in Beijing (China), Montréal (Canada), Vancouver (Canada), and Phoenix (USA).

2 Methodology

2.1 Single-Layer Urban Canopy Model

A schematic of the single-layer urban canopy model is shown in Fig. 1a; building arrays are represented as a two-dimensional and longitudinally infinite street canyon. To better capture the urban water cycle, we include the following hydrological processes: (1) evaporation from engineered pavements; (2) the energy and water balances of multilayer green roofs; (3) urban irrigation; (4) an anthropogenic heat flux; and (5) the urban oasis effect. A detailed description of each process is provided below. Compared to the current SLUCM scheme in the WRF model, the urban canopy model developed here explicitly accounts for surface heterogeneity. In particular, building roofs consist of green roofs and engineered roofs with different hydrothermal properties (Fig. 1b). The surface energy balance in the new Noah/SLUCM system is given by,

$$R_{\mathrm{n}} + Q_{\mathrm{F}} = LE + H + G, \tag{1}$$

where R_{n} is the net radiation, Q_{F} is the anthropogenic heat flux, LE, H and G are the latent, sensible and ground heat fluxes respectively. Specifically, the latent heat flux within a WRF urban grid cell consisting of both urban (impervious) and vegetation landscapes is computed as,

$$LE = (LE_{\mathrm{urb}} + Q_{\mathrm{ALH}})f_{\mathrm{urb}} + LE_{\mathrm{veg}}(1 - f_{\mathrm{urb}}), \tag{2}$$

$$LE_{\mathrm{veg}} = C_{\mathrm{H}}E_{\mathrm{p}}\alpha_{\mathrm{oasis}}, \tag{3}$$

$$LE_{\mathrm{urb}} = rf_{\mathrm{gr}}LE_{\mathrm{gr}} + r(1 - f_{\mathrm{gr}})LE_{\mathrm{r}} + (1 - r)LE_{\mathrm{g}} + 2hLE_{\mathrm{w}}, \tag{4}$$

where Q_{ALH} is the anthropogenic latent heat flux, f_{urb} is the fraction of urban landscape, subscripts urb, veg, gr, r, g, and w denote the urban landscape, vegetation landscape, green roof, roof, ground and wall respectively, E_{p} is the potential evaporation rate, C_{H} is a coefficient that accounts for the impacts of other variables on the evaporation, α_{oasis} is the oasis parameter, and dimensionless variables r and h represent the normalized roof width and building height respectively. LE_{urb} is calculated using the single-layer urban canopy model while LE_{veg} is computed using the Noah land-surface model.

2.2 Evaporation Over Paved Surfaces

In contrast to natural landscapes (soils and vegetation), engineered surfaces admit much simpler hydrological processes. As illustrated in Fig. 1b for a paved roof, a water-holding layer exists above the impervious datum due to the porosity of pavement. The layer also exists on wall and road surfaces, with water retained within this layer and acting as the source for evaporation. The latent heat flux over engineered pavements is given by (Wang et al. 2013),

$$LE = \frac{\delta}{d_{\mathrm{eng}}}\phi E_{\mathrm{p}}, \tag{5}$$

where ϕ is the porosity of engineered materials, d_{eng} is the maximum water-holding depth dependent on pavement materials, and δ is the water retention depth given by,

$$\phi\frac{\partial\delta}{\partial t} = \begin{cases} 0, & \text{if } \delta > d_{\mathrm{eng}} \\ \max(0,\, P - \phi E_{\mathrm{p}}), & \text{if } 0 \le \delta \le d_{\mathrm{eng}}, \quad P > 0 \\ P - \phi E_{\mathrm{p}}, & \text{if } 0 \le \delta \le d_{\mathrm{eng}}, \quad P \le 0 \end{cases}, \tag{6}$$

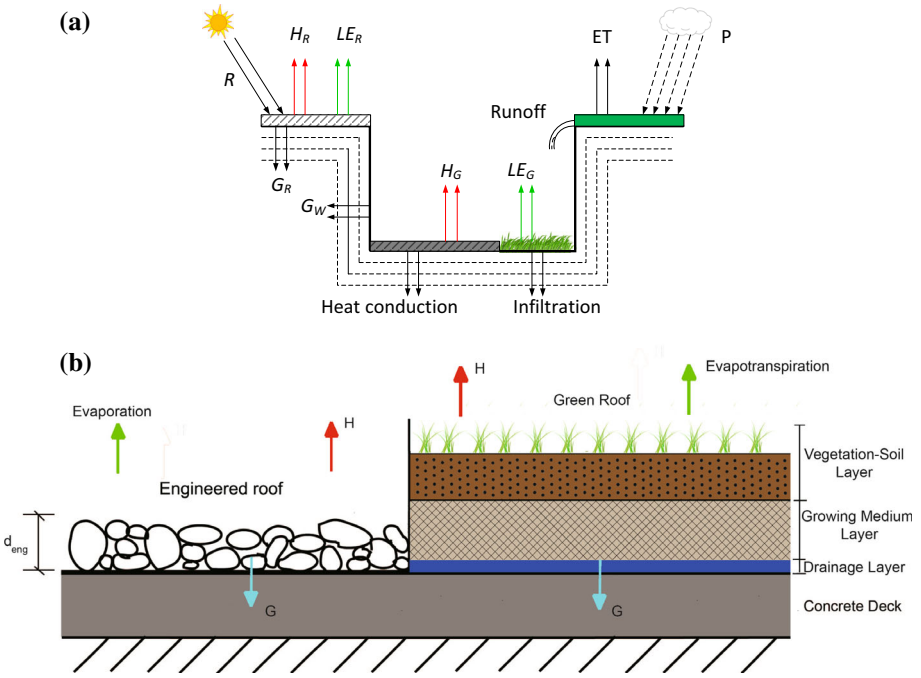

Fig. 1 Schematics for **a** the single-layer urban canopy model, and **b** a *green roof* and an engineered roof. Subscripts R, W, and G denote properties of roof, wall and ground, respectively; d_{eng} in (b) is the maximum water-holding depth of the paved surface

where P is the precipitation intensity. Previous studies have identified different values for d_{eng}; for example, Grimmond and Oke (1986) used a value of 0.59 mm to represent the retention capacity of impervious surfaces, while Ramamurthy and Bou-Zeid (2014) adopted a value of 1 mm for ground concrete and asphalt pavements. In this study, we set d_{eng} to be 1, 0.2 and 1 mm for engineered roof, wall and ground surfaces, respectively.

2.3 Water Balance of Multi-layer Green Roofs

A schematic of a multi-layer green roof system is shown in Fig. 1b. Compared to a conventional roof, it has three additional layers on top of the concrete deck, viz. the vegetation-soil, growing media and drainage layers. All three layers consist of porous materials and their volumetric water content θ is computed with vertical discretization. Temporal and spatial distributions of θ in the intermediate layers are given by the diffusive form of the Richards equation,

$$\frac{\partial \theta}{\partial t} = D(\theta)\frac{\partial^2 \theta}{\partial z^2} + \frac{\partial}{\partial z}K(\theta), \tag{7}$$

where $D(\theta)$ and $K(\theta)$ are the θ-dependent hydraulic diffusivity and conductivity respectively. Equation 7 is derived from Darcy's law assuming rigid, isotropic and homogeneous soils. The total latent heat flux from a green roof is then calculated from,

$$LE_{\text{gr}} = LE_{\text{dir}} + LE_{\text{c}} + LE_{\text{t}}, \tag{8}$$

where subscripts dir, c, and t represent direct evaporation from top soil layer, evaporation of precipitation intercepted by vegetation canopy and transpiration via vegetation. Details of these three components can be found in the community Noah land-surface model (Chen and Dudhia 2001). Within the green roof system, depths of the vegetation-soil layer and growing medium layer are strongly related to plant types and root depths, which can vary from about 0.05 m to more than 1 m depending on vegetation types (Dvorak and Volder 2010). For simplicity, here we use a constant thickness of 0.15 m for both the growing medium and soil-vegetation layers. The drainage layer is a thin layer constructed to transport drainage moisture away, and therefore its depth is not explicitly modelled.

2.4 Urban Irrigation

Several methods for estimating urban irrigation have been previously developed, including the use of field measurements, the minimum-month method, and the energy balance method (Mayer and Deoreo 1999; Senay et al. 2007). However, many of these are computationally expensive and inaccurate at the local or regional scale (Johnson and Belitz 2012). The impact of summertime irrigation was qualitatively discussed in previous studies for several cities, e.g. Beijing (Miao and Chen 2014), Phoenix (Diem and Brown 2003) and Vancouver (Grimmond and Oke 1986). Timing, duration and amount of irrigation vary from city to city and are subject to change according to vegetation type as well as local practices and regulations. Irrigation is therefore difficult to represent at the city scale. For simplicity, here we assume that urban irrigation is conducted for a 2-h period from 1800 to 2000 local time each day from May to September in all study cities. When irrigated, volumetric moisture of the top two soil layers (0.4 m thick) of urban lawns or green roofs is set to reach a threshold value of 0.33 where transpiration is not limited by water availability. Such treatment is used to broadly represent, rather than exactly match, urban irrigation schemes in a variety of cities. Development of a physically-based irrigation scheme remains an open challenge in urban hydroclimate modelling.

2.5 Anthropogenic Latent Heat Flux

The importance of anthropogenic heat in an urban area has been long recognized since the 1980s (Oke 1988; Grimmond 1992). To date, however, most studies have assumed that the anthropogenic heat is sensible in nature without accounting for the latent heat component. In the current Noah/SLUCM system, the anthropogenic heat flux is modelled as a fixed diurnal profile added to the sensible heat flux. Several recent studies suggested that water vapour emission by cooling systems constitutes a substantial portion of the latent heat flux in urban areas (Sailor et al. 2007; Miao and Chen 2014); in central Tokyo, this flux was shown to exceed $500\,\mathrm{W\,m^{-2}}$ during summer (Moriwaki et al. 2008). The diurnal variation of the anthropogenic latent heat flux follows the schedule of human activity and is relatively independent of season (Moriwaki et al. 2008), and this flux in the surface energy budget is given by,

$$Q_{\mathrm{ALH}} = Q_{\mathrm{ALHMAX}} f_{\mathrm{ALH}}, \tag{9}$$

where Q_{ALHMAX} is the daily maximum anthropogenic latent heat flux dependent on the season and f_{ALH} is a diurnally-varying coefficient. Miao and Chen (2014) developed a diurnal profile of f_{ALH} for the Beijing metropolitan area based on the predicted *LE* from the Noah/SLUCM modelling system and meteorological observations. Their diurnal profile matches daily human activities and is similar to that of Tokyo derived by Moriwaki et al.

(2008). We adopt this profile to represent the general diurnal variability of the urban anthropogenic latent heat flux and apply it to Vancouver, Montréal and Phoenix in subsequent simulations. Q_{ALHMAX} is estimated to be 17.0, 41.9, 24.4 and 18.0 $\mathrm{W\,m^{-2}}$ for spring, summer, autumn and winter in Beijing respectively (Miao and Chen 2014). In Vancouver, the monthly average anthropogenic latent heat flux is estimated using a top-down methodology developed by Sailor and Lu (2004).

Seasonal anthropogenic latent heat-flux data are not available for Phoenix and Montréal, although previous studies have estimated daily maximum anthropogenic heat-flux values for Montréal (Lemonsu et al. 2010) and Phoenix (Sailor and Hart 2006). Here, we adopt the approach of Bateni and Entekhabi (2012) and partition the total anthropogenic heat into sensible and latent heat-flux components in the Noah/SLUCM system. Given a small temperature perturbation, based on a linear stability analysis that restores the land surface to thermodynamic equilibrium, the ratio of anthropogenic latent heat flux to sensible heat flux is computed as,

$$\frac{Q_{\mathrm{ALHMAX}}}{Q_{\mathrm{ASHMAX}}} = \beta\frac{\Delta}{\gamma}, \tag{10}$$

$$Q_{\mathrm{ALHMAX}} + Q_{\mathrm{ASHMAX}} = Q_{\mathrm{AHMAX}}, \tag{11}$$

where Q_{AHMAX} is the daily maximum anthropogenic heat flux, Q_{ASHMAX} is the daily maximum anthropogenic sensible heat flux, Δ is the slope of the saturation vapour pressure curve, γ is the psychrometric constant, and β is the moisture availability parameter: $\beta = 0$ for completely dry surfaces and $\beta = 1$ for a saturated surface. Yang et al. (2013) evaluated the method against field measurements over lake, vegetation, and suburban land surfaces, finding that a reasonable choice of β is $\approx$0.5 in autumn and $\approx$1.5 in summer over a vegetated surface. The value of $\beta > 1$ in summer because of the additional transpiration process for urban vegetation. Assuming the latent heat flux over impervious surfaces is negligible in the absence of rainfall, moisture availability for the city is calculated using,

$$\beta = \beta_{\mathrm{veg}}(1 - f_{\mathrm{urb}}), \tag{12}$$

where β_{veg} is set as 1.0, 1.5, 0.5 and 0.2 for spring, summer, autumn, and winter, respectively. This method, albeit not exact, provides a usable scheme for estimating anthropogenic sensible and latent heat fluxes where detailed observations are not available.

2.6 Urban Oasis Effect

The urban oasis effect on plant transpiration rate has been addressed in several field experiments; a schematic of this effect is shown in Fig. 2. Without obstacles to radiation receipt and airflow, patchy vegetation in urban areas has higher rates of potential evapotranspiration than does large area vegetation in the natural environment. Oke (1979) found that the actual evapotranspiration from an irrigated suburban lawn was about 1.3 times greater than that from an irrigated rural pasture. Hagishima et al. (2007) conducted experiments using 203 nearly homogeneous potted plants and concluded that scattered small plants had a transpiration rate about 1.6 times that of large vegetation. Miao and Chen (2014) used meteorological observations with the Noah/SLUCM modelling system and obtained an oasis parameter of about 1.5 for Beijing. Here we adopt a value of 1.5 to account for the oasis effect on potential evapotranspiration rate for urban vegetation.

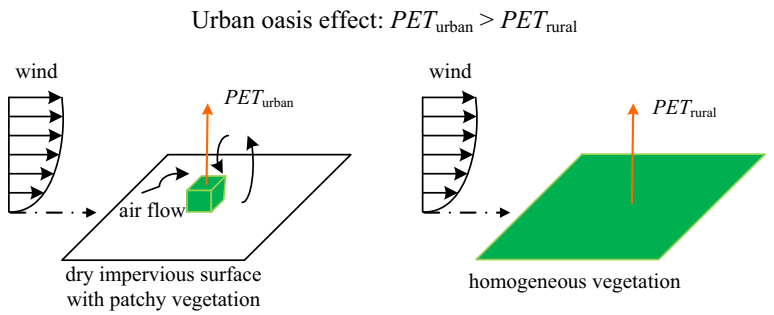

Fig. 2 Schematics for oasis effect: comparing potential evapotranspiration (*PET*) over vegetated surfaces in urban and rural areas

3 Site Description

To evaluate the enhanced Noah/SLUCM modelling system, flux measurements were collected from eddy-covariance towers in four metropolitan areas, viz. Beijing, Phoenix, Vancouver and Montréal. Basic meteorological quantities—wind speed, wind direction, air temperature and relative humidity—were also measured at these sites. In the Beijing metropolitan area, three-level flux observations were made at heights 47, 140 and 280 m on the Chinese Academy of Science 325-m Meteorological and Environmental Observation tower (Miao et al. 2012). Footprint analysis by Wang et al. (2009) demonstrated that the flux measurement at 140 m covered a major fraction of the Beijing metropolitan area (20 km × 20 km. For Vancouver and Montréal, datasets were acquired from the Environmental Prediction in Canadian Cities (EPiCC) network (http://www.epicc.ca), which conducted measurements to evaluate the urban meteorological numerical systems used at the Meteorological Service of Canada. Here we use data from the Vancouver Sunset tower location and the Montréal urban residential site. More details can be found in Bergeron and Strachan (2012) for the Montréal site, and in Tooke et al. (2009) and van der Laan et al. (2011) for Vancouver. In Phoenix, observations were obtained from the eddy-covariance tower deployed at Maryvale, west Phoenix, through the Central Phoenix Project Long Term Ecological Research program. The local scale surface energy balance for the area has been obtained for the entire calendar year 2012 (Chow et al. 2014).

4 Model Evaluation and Discussion

Here we present simulation results from the Noah/SLUCM system with enhanced modelling of urban hydrological processes, compared against observational datasets collected at the four aforementioned metropolitan areas. Hereafter, we refer to the current Noah/SLUCM system as the old SLUCM, and the version with the proposed hydrological processes included as the new SLUCM. In this study, models are run in an offline (stand-alone) mode, with simulations driven by 30-min averaged meteorological data obtained from eddy-covariance towers, including wind speed, wind direction, air temperature, relative humidity, atmospheric pressure, incoming shortwave and longwave radiative fluxes, and precipitation. Without information on the large-scale deployment of green roofs in any of these study cities during the measurement periods, simulations are performed with zero green roof fraction.

Table 1 Urban canopy parameters and simulation periods for study metropolitan areas

Input parameters	Unit	Phoenix	Beijing	Vancouver	Montréal
h (building height)	m	7.5[a]	18.3[d]	4.9[e]	8.35[f]
l_{roof} (roof width)	m	9.4[a]	10[a]	12.3[e]	14[f]
l_{road} (road width)	m	9.4[a]	10[a]	9.4[a]	25.2[f]
f_{urb} (urban fraction)	–	0.844[b]	0.783[d]	0.68[e]	0.72[f]
α_R (albedo of roof)	–	0.16	0.2	0.1	0.12
α_W (albedo of wall)	–	0.16	0.2	0.1	0.12
α_G (albedo of road)	–	0.16	0.2	0.1	0.12
Q_{AHMAX}	W m^{-2}	10.3[c]	*[1]	*[2]	24.0[g]
Vegetation	–	Shrubland/grassland	Cropland/grassland	Shrubland/grassland	Shrubland/grassland
Simulation period	–	17 April 2012–31 December 2012	30 June 2009–30 June 2010	22 January 2009–31 October 2009	3 April 2009–31 August 2009[#]
Spring	–	17 April 2012–31 May 2012	1 March 2010–31 May 2010	1 March 2009–31 May 2009	3 April 2009–23 April 2009
Summer	–	1 June 2012–31 August 2012	1 July 2009–31 August 2009	1 June 2009–31 August 2009	1 June 2009–31 August 2009[#]

[a] Default values prescribed in Noah/SLUCM
[b] Myint et al. (2011)
[c] Sailor and Hart (2006)
[d] Wang et al. (2009)
[e] Goodwin et al. (2009)
[f] Lantz and Wang (2010)
[g] Lemonsu et al. (2010)
*[1] Seasonal data of anthropogenic latent heat flux available from Miao and Chen (2014)
*[2] Seasonal data of anthropogenic latent heat flux available from Sailor and Lu (2004)
[#] Gap exists due to data availability during the simulation period

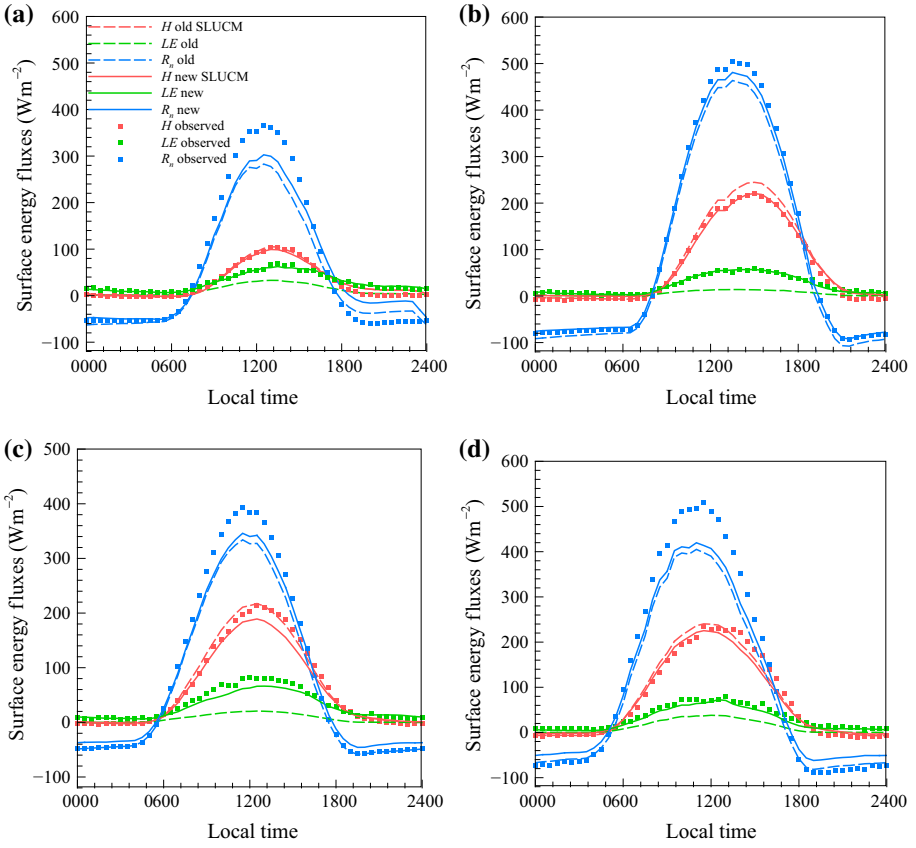

Fig. 3 Averaged diurnal profiles of modelled and observed H, LE and R_n for **a** Beijing, **b** Phoenix, **c** Vancouver and **d** Montréal

Performance of the Noah/SLUCM system and coupled hydrological processes relies heavily on the accurate determination of input parameters (Loridan et al. 2010; Wang et al. 2011b; Yang and Wang 2014). As field measurements of all input parameters of the model are rarely possible, here we only collect sensitive parameters of the model. Loridan et al. (2010) performed an extensive evaluation of the Noah/SLUCM system and found that the latent heat flux is most sensitive to the vegetation fraction. In Beijing, land-cover and building characteristics have been reported by Wang et al. (2009). Urban land-surface parameters were obtained from high resolution lidar data for Vancouver (Goodwin et al. 2009), and from satellite imagery as well as public Geographic Information System data for Montréal (Lantz and Wang 2010). In Phoenix, Myint et al. (2011) developed a set of multi-scale decision rules and supervised approaches using an object-based classifier, and achieved an overall accuracy higher than 90 % in urban land-cover classification. This method is employed to acquire the vegetation fraction of a 1 km × 1 km area centred at the eddy-covariance tower in Phoenix. At each site, the area-averaged albedo is estimated from measured incoming and outgoing shortwave radiative fluxes during a diurnal cycle on a summer clear day. Facet albedo values are then assigned (i.e., for roof, wall and ground) to achieve the correct overall surface albedo.

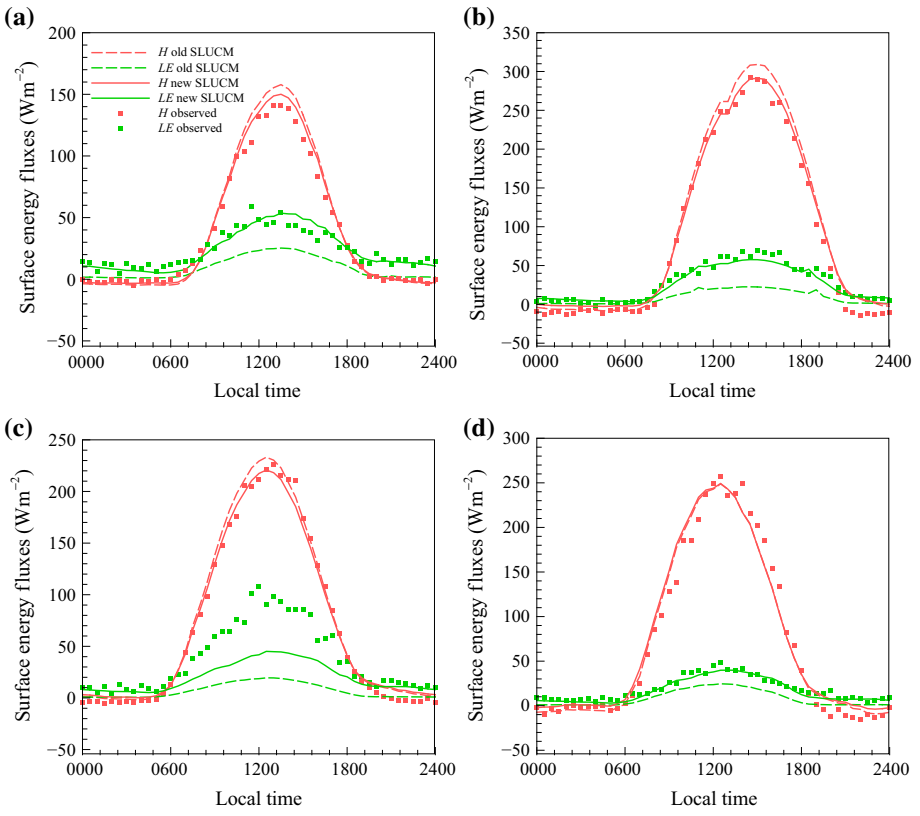

Fig. 4 Averaged diurnal profiles of modelled and observed H and LE in spring for **a** Beijing, **b** Phoenix, **c** Vancouver and **d** Montréal

In addition to those obtained from field analysis, default values are used for the remaining parameters. Currently, urban canopy parameters are prescribed in the Noah/SLUCM system for three urban land-use categories: low-density residential, high-density residential, and industrial and commercial. We use the industrial and commercial category to represent the Beijing study site, and the high-density residential category for Phoenix, Montréal and Vancouver. Properties of different vegetated surfaces are also prescribed in the model. Based on results from Loridan et al. (2010), we select the cropland/grassland category to represent the urban vegetation for Beijing, and the mixed shrubland/grassland category for Phoenix, Montréal and Vancouver. Urban canopy parameters and simulation periods for the four study sites are summarized in Table 1. Due to limited data availability, the simulation for Montréal is only run for 20 and 35 days during spring and summer 2009, respectively.

Model predictions and field observations of H, LE and R_n are compared in Fig. 3. Located in a semi-arid region, Phoenix has a smaller latent heat flux compared to the other three metropolitan areas. It is clear from Fig. 3 that, due to the lack of realistic urban hydrological processes, the old SLUCM significantly underestimates LE with a discrepancy of more than 40 W m^{-2} at 1400 local time. With the incorporation of urban hydrological processes, the new SLUCM is able to predict LE with improved accuracy as compared to field measurements, with a deviation of $<$10 W m^{-2} at 1400 local time for all study areas. Constrained by the

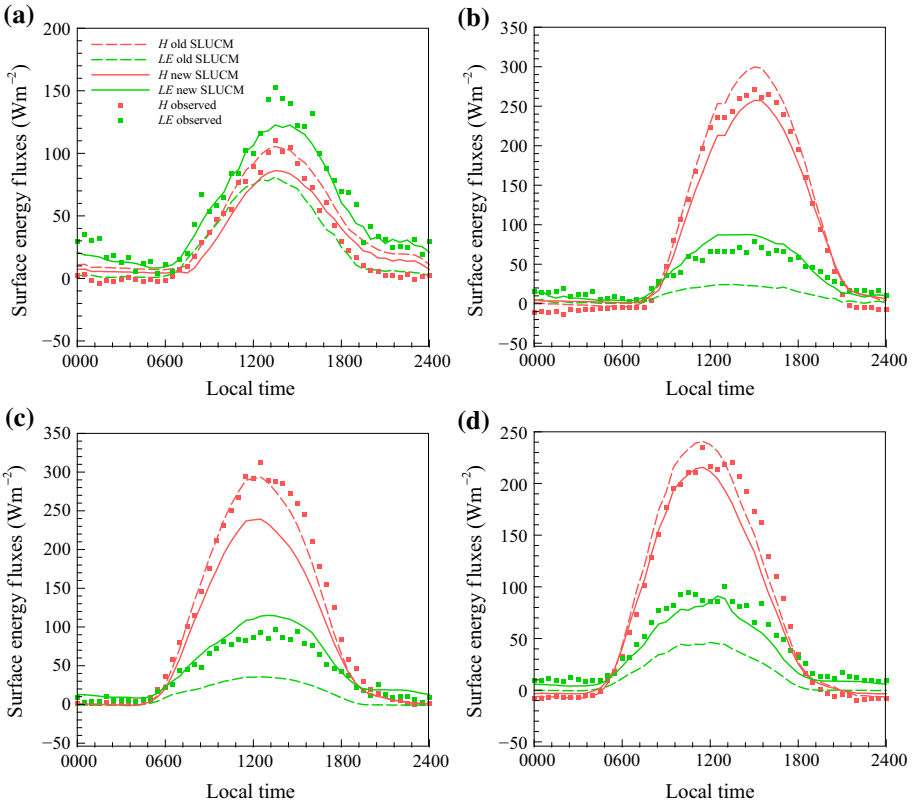

Fig. 5 Averaged diurnal profiles of modelled and observed H and LE in summer for **a** Beijing, **b** Phoenix, **c** Vancouver and **d** Montréal

surface energy balance, the increase in LE in the new SLUCM leads to less available energy for H and G, and it is found that (not shown here) about 70 % of the reduction is redistributed to H. This implies that the inclusion of hydrological processes in the model has an important impact on the partitioning of available energy into turbulent fluxes, without significantly altering the soil thermal storage. Figure 3 also illustrates that the incorporation of hydrological processes also improves the prediction of daytime net radiation, leading to improved estimates of the daytime surface temperature by the new SLUCM. In addition, the surface energy residual ($R_n + Q_F - H - LE - G$) is calculated over the entire simulation period. Mean residuals for all study sites are less than 0.15 W m^{-2}, indicating the surface energy balance is maintained after the incorporation of hydrological processes.

Considering the seasonal variation of urban irrigation, we further evaluate model results against observations at the intra-annual scale. Results from spring and summer periods are plotted in Figs. 4 and 5, respectively. The predicted LE by the new SLUCM is in good agreement with field observations (with absolute error $<$30 W m^{-2}) except that a substantial deviation of 60 W m^{-2} is found at Vancouver in spring. It is noteworthy that Vancouver has a larger LE in spring than in summer due to high precipitation; the opposite is found in the other three cities. This discrepancy in spring is possibly related to specific missing hydrological processes in the current model, e.g. snow melting, necessitating a continuous improvement

Table 2 Summary of the median, maximum, minimum, 25th and 75th percentile of the *RMSE* (W m^{-2}) between model prediction and observation

Site	Statistics	Old SLUCM			New SLUCM		
		H	*LE*	R_n	*H*	*LE*	R_n
Beijing	Median	2.3	13.5	21.0	4.3	2.7	29.6
	Minimum	0.0	4.6	1.5	0.0	0.1	0.3
	25th percentile	1.2	9.6	7.2	1.3	0.6	5.5
	75th percentile	7.1	21.3	51.6	8.0	4.4	44.1
	Maximum	13.3	37.9	93.7	13.3	7.6	67.4
Phoenix	Median	10.6	11.5	13.1	6.1	1.8	4.5
	Minimum	1.3	1.3	4.1	0.4	0.0	0.0
	25th percentile	5.2	5.7	9.4	4.3	0.8	3.7
	75th percentile	19.4	31.5	30.7	9.2	2.3	11.7
	Maximum	31.8	45.8	42.7	15.3	10.2	14.6
Vancouver	Median	3.3	17.4	3.2	3.9	3.8	11.8
	Minimum	0.0	5.1	0.0	0.0	0.1	1.1
	25th percentile	1.4	8.3	0.6	2.1	1.7	9.7
	75th percentile	10.1	47.2	39.2	14.0	11.1	25.7
	Maximum	17.6	62.5	58.3	33.3	20.7	47.8
Montréal	Median	7.3	15.5	12.6	7.2	5.0	26.7
	Minimum	0.0	6.6	0.3	1.5	0.1	1.2
	25th percentile	2.5	9.1	6.9	4.2	3.3	20.3
	75th percentile	17.7	31.1	73.2	12.4	8.4	56.0
	Maximum	32.6	42.0	111.9	42.5	17.0	96.1

of the WRF–urban modelling system in the future. During summer, the increase of *LE* is about 100 % larger than that in spring due to irrigation in the model; the accuracy of the prediction of *LE* is notably improved at all study sites. Nevertheless, a significant deviation in *H* is observed in Vancouver, which is up to $\approx$50 W m^{-2} around noon. In general, Figs. 4 and 5 show that the new SLUCM is capable of reproducing seasonal patterns of turbulent heat fluxes for the study cities except Vancouver.

To quantitatively assess the impact of the proposed hydrological processes, the root-mean-square error (*RMSE*) between observed and modelled results is computed for the entire simulation period. The statistics are summarized in Table 2, and are presented in Fig. 6 to facilitate the visualization of the results. Despite the locations, the *RMSE* from the new SLUCM is notably smaller than that from the old SLUCM with respect to *LE*. Averaged median *RMSE* values for the four study sites are 15 and 3 W m^{-2} for the old and new SLUCM, respectively. With respect to *H*, the old SLUCM has good overall performance for all study sites, with a median *RMSE* of 6 W m^{-2}; the model performance is slightly better for Beijing and Vancouver, and much improved for Montréal and Phoenix in terms of the maximum *RMSE*. In addition, the averaged median *RMSE* for *H* and *LE* for the new SLUCM is 5 and 3 W m^{-2}, respectively, which are significantly better than the corresponding median *RMSE* of 22 and 26 W m^{-2} averaged over the group of 32 urban energy balance models at the final stage (where all urban canopy models were fine-tuned using most detailed field parameters) (Grimmond et al. 2011).

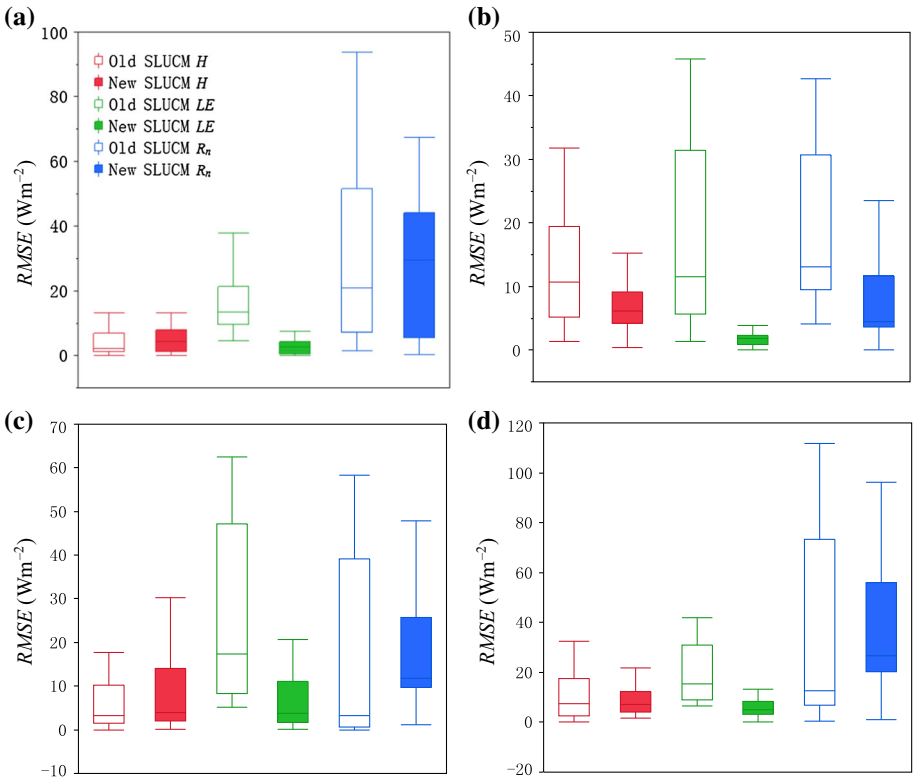

Fig. 6 Box plots of *RMSE* between observed and model predicted H, LE and R_n for **a** Beijing, **b** Phoenix, **c** Vancouver and **d** Montréal. *Top* and *bottom of the box* represent the 75th and 25th percentile, the *horizontal line* indicates the median, *top* and *bottom bars* are the maximum and minimum values, respectively

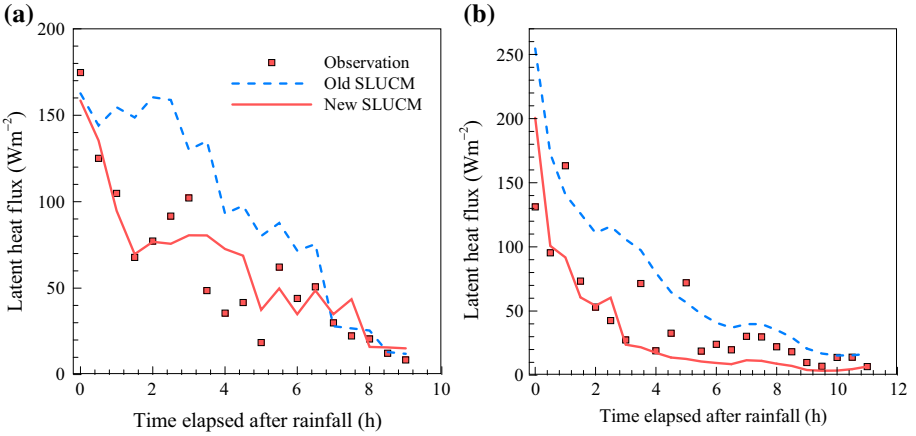

Fig. 7 Averaged *LE* after rainfall events during a summer period from two evaporation parametrization schemes for **a** Beijing during 30 June–30 August 2009 (averaged over four major rainfall events), and **b** Phoenix during 3 July–31 August 2012 (averaged over four major rainfall events)

From Figs. 3, 4, 5 and 6 it is evident that the major improvement of the new SLUCM is in its capability of predicting *LE*, as a result of the enhanced physical representation of urban hydrological processes. Among the proposed hydrological processes, evaporation over pavement surfaces only takes effect during and shortly after precipitation due to the low water-holding capacity. Considering the substantial fraction of paved surface in urban areas, we specifically focus on *LE* during rainfall periods to examine the impact of different parametrization schemes. The Noah/SLUCM modelling system is run with the old (empirical decay function by Miao and Chen 2014) and new (resolving water-holding layer in this study) schemes respectively. Figure 7 shows the results of the comparison for summer in Beijing and Phoenix, where it is clear that the old parametrization scheme overestimates *LE* after the onset of rainfall. Large differences are observed throughout the period with a maximum error of about $80\,\mathrm{W\,m^{-2}}$ in Beijing and about $120\,\mathrm{W\,m^{-2}}$ in Phoenix. In contrast, the new evaporation scheme (Eq. 6) yields more realistic predictions of *LE* with better agreement with field measurements, with maximum errors <40 and $70\,\mathrm{W\,m^{-2}}$ in Beijing and Phoenix, respectively. This new parametrization scheme for engineered surfaces can markedly improve the prediction of *LE*, and consequently improve the representation of the urban water cycle during and after rainfall events.

Furthermore, for each hydrological process proposed herein, the relative contribution is calculated as the ratio (percentage) between the change of *LE*, by removing the particular process, and the overall change of *LE* by including all hydrological processes. It is found that evaporation over engineered pavements has the least relative contribution ($<0.1\,\%$), because it is only effective during and shortly after precipitation. The relative contribution from irrigation varies from about 7 % in Beijing to about 69 % in Phoenix. The oasis effect contributes more ($>10\,\%$) to the overall *LE* changes in Phoenix, Vancouver and Montréal, than that in Beijing. It is mainly because the urban cropland/grassland (Beijing) has a higher actual rate of evapotranspiration limited by available energy (i.e. supply) rather than the potential rate (i.e. atmospheric demand). The anthropogenic latent heat flux is determined by population density and the urban category of the measurement site. Therefore its contribution varies vastly for different cities, ranging from about 0.5 % in Vancouver to about 50 % in Beijing.

5 Green Roof Simulations

Here the new Noah/SLUCM model is applied to explore the effect of green roof systems on urban hydroclimate, especially on the modification of the surface water and energy budgets. We use five scenarios with different green roof fractions, viz. zero, 25, 50, 75, and 100 % of the total roof area. Simulations are conducted for a five-day period in mid-summer for the four study cities: Beijing, (June 19–24 2010), Phoenix (July 5–10 2012), Vancouver (July 16–21 2009), and Montréal (June 2–7 2009), driven by the observed meteorological forcing. The selected periods were characterized by clear-sky conditions with no precipitation, while the initial soil moisture of green roofs is assumed to be the same as that of the ground vegetation. Note that urban irrigation is used for subsequent simulations; therefore model results represent the maximum (potential) capacity of evaporative cooling and energy saving for green roofs.

The predicted surface temperature (T_s), sensible and latent heat fluxes with different green roof area fractions are shown in Figs. 8, 9 and 10. With increased green roof fraction, and therefore a stronger evaporative cooling effect, urban T_s and *H* decrease while *LE* increases, as expected. Figures 8, 9 and 10 demonstrate the range of modelled T_s, *H*, and *LE* that

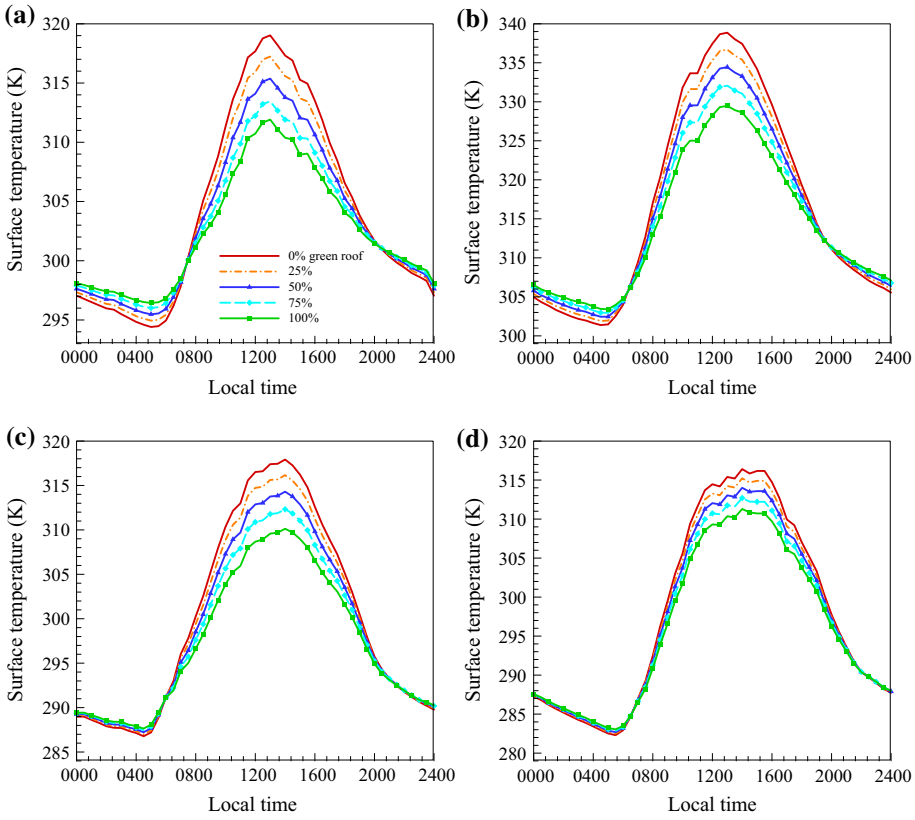

Fig. 8 Model predicted T_s with various *green roof* fractions during a 5-day summer period for **a** Beijing, **b** Phoenix, **c** Vancouver and **d** Montréal

rooftop modification can produce in each city. Replacing 25 % of the rooftop with green roofs reduces the daily peak T_s by 1–2 K in study areas, while if green roofs are implemented over the entire city, the reduction in the daily peak T_s can be up to 5–10 K, consistent with values reported by Santamouris (2014). Compared to Beijing and Montréal, Phoenix and Vancouver have larger reductions in T_s; in Phoenix, the reduction is partly due to the presence of a larger roof fraction (see Table 1), which provides a greater area for green roof systems. In addition, the dry atmosphere in the semi-arid environment in Phoenix induces higher potential evapotranspiration, which in turn leads to more significant cooling. Vancouver, though its urban fraction is the lowest among all study cities, has the highest roof- to urban-area ratio, leading to more effective cooling per unit urban area by green roofs. Greater available energy at the surface, as a result of greater incoming solar radiation in Phoenix and a lower albedo in Vancouver, also contributes significantly to larger increases in *LE* and reductions in T_s in the two cities.

Figure 9 shows that green roofs are capable of substantially reducing the sensible heat flux in urban areas. As H is closely related to the difference between the surface and air temperatures, the magnitude of reduction in H follows the trend in the reduction in T_s. Installation of green roofs over the entire available rooftop area can decrease the daily peak H by about 100 W m^{-2} in Beijing and Montréal, and about 160 W m^{-2} in Phoenix and Vancouver. At

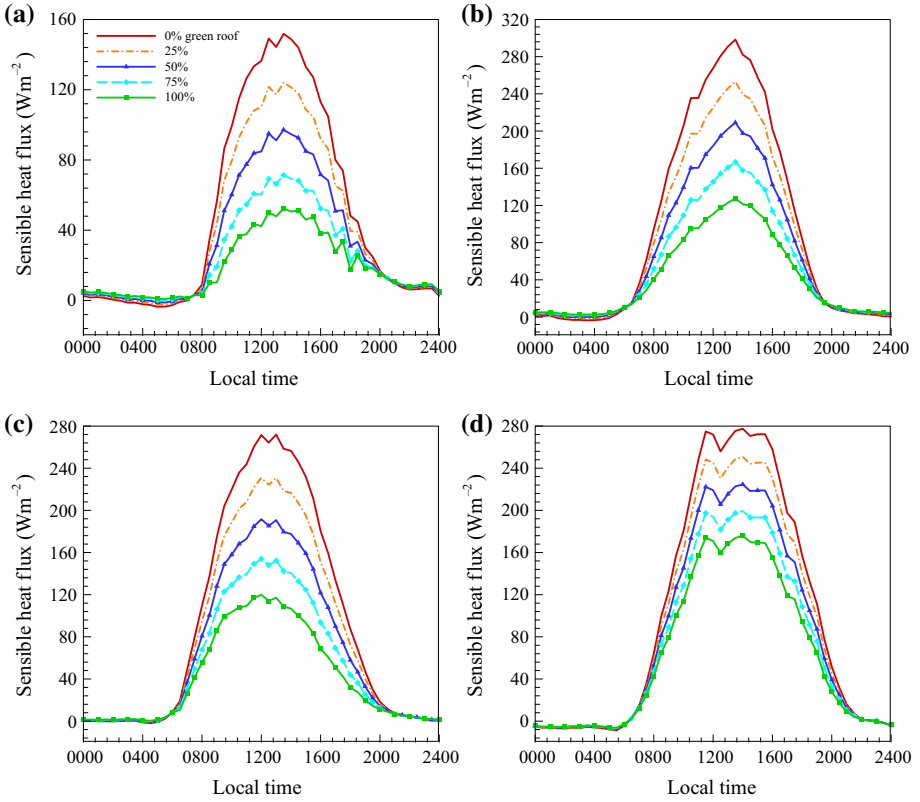

Fig. 9 Model predicted H with various *green roof* fractions during a 5-day summer period for **a** Beijing, **b** Phoenix, **c** Vancouver and **d** Montréal

night, the cooling effect becomes insignificant as the energy source for evaporation, i.e. solar radiation, vanishes. Due to the larger heat capacity of moist soils as compared to pavement materials, nighttime T_s and H for green roofs are higher than conventional roofs. The warming effect of green roofs at night is more evident in low-latitude areas that accumulate more thermal energy during daytime. Among the study cities, the nighttime warming (as compared to the case without green roofs) is <1 K in Vancouver and Montréal, but can be >2 K in Beijing and Phoenix. Overall, the nighttime temperature increase is much smaller than the daytime temperature reduction.

In addition, green roofs can lead to an increase of more than 70 W m^{-2} in peak LE values in all four cities (Fig. 10), up to 130 W m^{-2} in Phoenix. It is noteworthy that the increase in LE is relatively linear when the green roof fraction rises from zero to 75 %, consistent with an earlier result (Yang and Wang 2014). However, as the green roof fraction increases from 75 to 100 %, the increment of LE becomes much smaller, revealing a complex mechanism of surface energy partitioning for green roof systems in this range. On the one hand, the decreased H due to surface cooling contributes more available energy for evapotranspiration (LE increases), whereas the associated reduction in buoyancy weakens the turbulent mixing and more moisture retained at the surface (LE decreases). Results in Fig. 10 indicate the

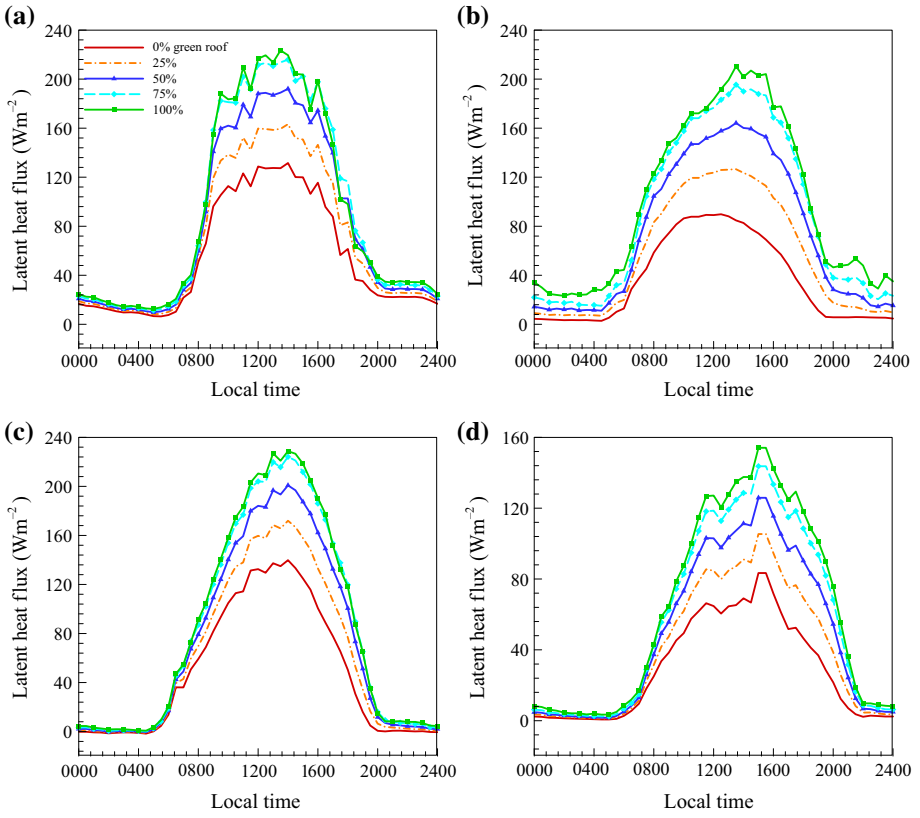

Fig. 10 Model predicted *LE* with various *green roof* fractions during a 5-day summer period for **a** Beijing, **b** Phoenix, **c** Vancouver and **d** Montréal

existence of a threshold capacity, beyond which further increasing green roof fraction will have a negligible effect on *LE*.

Moreover, the cooling effect by green roofs in turn leads to the saving of energy consumption of buildings, especially in summers. To assess the impact of green roofs on the building energy consumption, we calculate the heat flux conducted into the building through the roof (Q_{in}). A roof thermal insulation value of $R30$ is used in all simulations. Model predicted Q_{in} with different green roof area fractions in various cities are shown in Fig. 11 for the summer period. The peak Q_{in} occurs around 1800 local time, whereas the daily peak T_{s} occurs at about 1400 local time. The time lag of about 4 h implies the temporal gap between the hottest time and the largest cooling demands of buildings (Wang 2014b). During the study period, diurnal peak Q_{in} values without green roofs are $>15\,\text{W}\,\text{m}^{-2}$ at all study areas, up to $50\,\text{W}\,\text{m}^{-2}$ in Phoenix. With green roofs, Q_{in} can be reduced to nearly zero throughout the day in Vancouver and Montréal, and to $<7\,\text{W}\,\text{m}^{-2}$ in Beijing and Phoenix, implying significant potential saving of building cooling energy in summer.

To illustrate the impact of green roofs on building energy consumption in cool seasons, a second set of 5-day simulations (different from previous simulation periods in mid-summer) were conducted for Vancouver (March 8–13 2009), Phoenix (December 6–11 2012), Beijing (January 20–25 2010), and Montréal (April 6–11 2009). In Fig. 12, diurnal profiles of Q_{in}

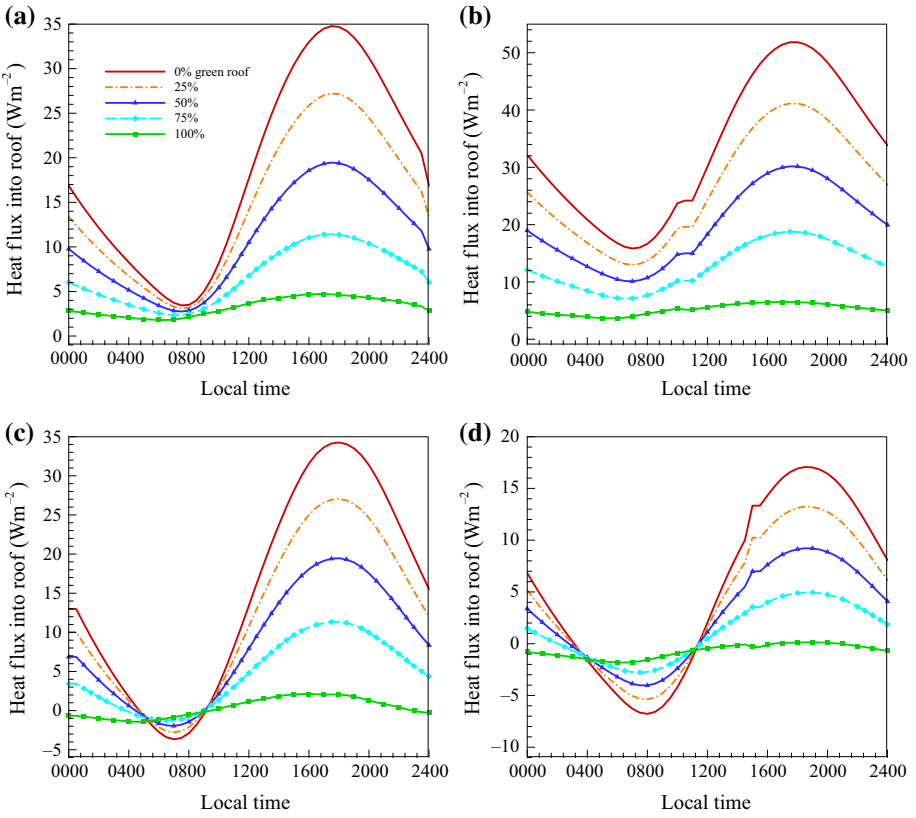

Fig. 11 Model predicted Q_{in} with various green roof fractions during a 5-day summer period for **a** Beijing, **b** Phoenix, **c** Vancouver and **d** Montréal

exhibit a similar trend to those in summer, where negative values indicate outward heat fluxes with a heating demand for building interiors. During the simulation period, the highest peak Q_{in} of $-18\,\text{W}\,\text{m}^{-2}$ and the lowest peak Q_{in} of $-43\,\text{W}\,\text{m}^{-2}$ are observed in Phoenix and Beijing, respectively. Implementation of green roofs can increase these peaks to about -4 and $-9\,\text{W}\,\text{m}^{-2}$ in corresponding cities, suggesting a considerable saving of heating loads. This demonstrates that the insulation effect of additional layers in a green roof system is important in improving building energy efficiency in cool-to-cold climates.

6 Concluding Remarks

We implemented physical urban hydrological parametrizations into the integrated Noah/SLUCM modelling system, including (1) an anthropogenic latent heat flux, (2) urban irrigation, (3) the urban oasis effect, (4) evaporation over engineered pavements, and (5) multilayer green roofs. Comparisons against field measurements show that the enhanced Noah/SLUCM system has improved accuracy in predicting turbulent fluxes over urban areas, especially the latent heat flux. The new model is able to capture not only the diurnal cycle but also intra-annual variations of H and LE in various cities. With the parametrization of

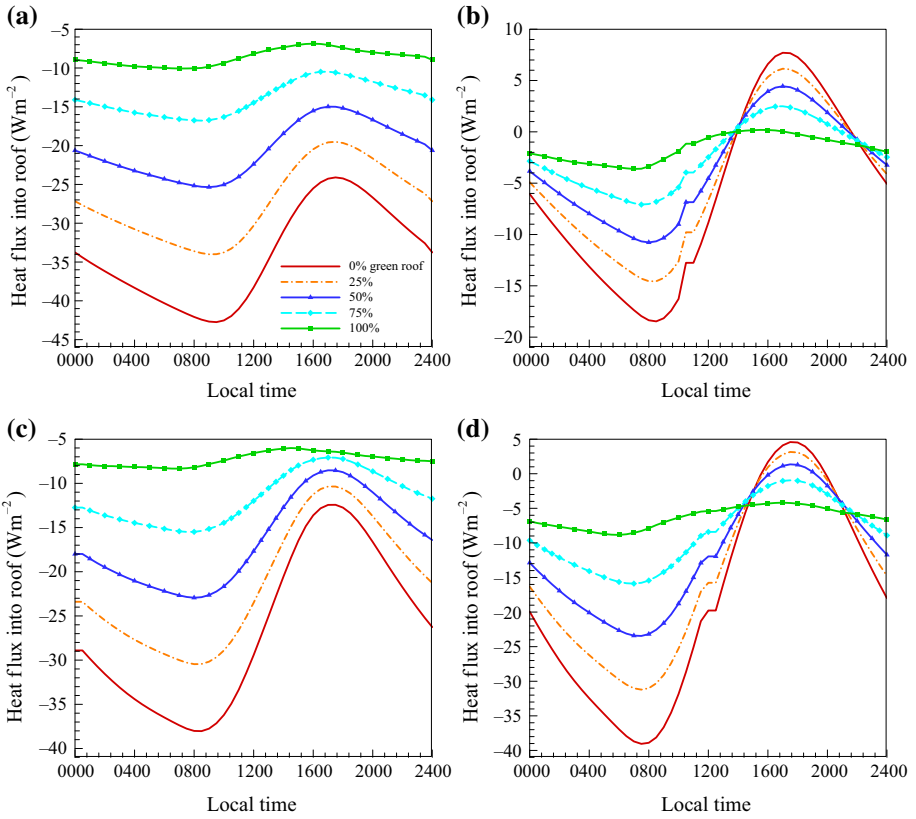

Fig. 12 Model predicted Q_{in} with various green roof fractions during a 5-day period for **a** Beijing from January 20–25 2010, **b** Phoenix from December 6–11 2012, **c** Vancouver from March 8–13 2009 and **d** Montréal from April 6–11 2009

water holding capacity of paved surfaces, actual *LE* is better predicted during and shortly after rainfall periods. Hence the new Noah/SLUCM model improves the predictive skills of the coupled WRF-urban modelling system, and provides more accurate lower boundary conditions for land–atmosphere interactions. In particular, the implementation of green roofs is shown to be effective in mitigating the urban heat island effect and improving building energy efficiency.

In general, results of the new Noah/SLUCM modelling system are promising, even with a large number of default urban parameters, as prescribed in the WRF model. Nevertheless, for specific cities, e.g. Vancouver, the presence of model-measurement differences requires more meticulous determination of model uncertainty as well as input parameters. Representing vegetation with a tile approach in the Noah/SLUCM system, where interactions between built and vegetated surfaces in urban canyons are neglected, may also contribute to errors in predictions. An integrated multi-level vegetation parametrization may have potential for further improvements, though a previous review (Grimmond et al. 2011) showed a comparative performance between urban canopy models using tile and integrated approach. In addition, the lack of snow/ice hydrology in current urban modelling systems necessitates further devel-

opment of physically-based urban parametrization schemes, especially those related to the coupled energy–water transport mechanisms.

Acknowledgments This work is supported by the National Science Foundation (NSF) under grant number CBET-1435881. Partial financial supports for ZHW and JY from the Central Arizona-Phoenix Long-Term Ecological Research project under NSF grant CAP3: BCS-1026865, and the Summer Visitor's program by the National Center for Atmospheric Research are gratefully acknowledged. SM is supported by the National Natural Science Foundation of China under grant No. 41175015.

References

Arnfield AJ (2003) Two decades of urban climate research: a review of turbulence, exchanges of energy and water, and the urban heat island. Int J Climatol 23:1–26

Bateni SM, Entekhabi D (2012) Relative efficiency of land surface energy balance components. Water Resour Res 48:W04510

Bergeron O, Strachan IB (2012) Wintertime radiation and energy budget along an urbanization gradient in Montreal, Canada. Int J Climatol 32:137–152

Chen F, Dudhia J (2001) Coupling an advanced land surface-hydrology model with the Penn State-NCAR MM5 modeling system. Part I: Model implementation and sensitivity. Mon Weather Rev 129:569–585

Chen F, Kusaka H, Tewari M, Bao JW, Hirakuchi H (2004) Utilizing the coupled WRF/LSM/Urban modeling system with detailed urban classification to simulate the urban heat island phenomena over the Greater Houston area. In: Fifth symposium on the urban environment, Vancouver, Canada, 23–27 August 2004

Chen F, Kusaka H, Bornstein R, Ching J, Grimmond CSB, Grossman-Clarke S, Loridan T, Manning KW, Martilli A, Miao SG, Sailor D, Salamanca FP, Taha H, Tewari M, Wang XM, Wyszogrodzki AA, Zhang CL (2011) The integrated WRF/urban modelling system: development, evaluation, and applications to urban environmental problems. Int J Climatol 31:273–288

Chow WT, Volo TJ, Vivoni ER, Jenerette GD, Ruddell BL (2014) Seasonal dynamics of a suburban energy balance in Phoenix, Arizona. Int J Climatol (published online). doi:10.1002/joc.3947

Diem JE, Brown DP (2003) Anthropogenic impacts on summer precipitation in central Arizona, USA. Prof Geogr 55:343–355

Dvorak B, Volder A (2010) Green roof vegetation for North American ecoregions: a literature review. Landsc Urban Plan 96:197–213

Field CB, Barros VR, Mach K, Mastrandrea M (2014) Climate change 2014: impacts, adaptation, and vulnerability. Working Group II Contribution to the IPCC 5th Assessment Report—Technical Summary, 76 pp

Goodwin NR, Coops NC, Tooke TR, Christen A, Voogt JA (2009) Characterizing urban surface cover and structure with airborne LIDAR technology. Can J Remote Sens 35:297–309

Grimmond CSB (1992) The suburban energy balance: methodological considerations and results for a mid-latitude west coast city under winter and spring conditions. Int J Climatol 12:481–497

Grimmond CSB, Oke TR (1986) Urban water balance: 2. Results from a suburb of Vancouver, British Columbia. Water Resour Res 22:1404–1412

Grimmond CSB, Blackett M, Best MJ, Barlow J, Baik JJ, Belcher SE, Bohnenstengel SI, Calmet I, Chen F, Dandou A, Fortuniak K, Gouvea ML, Hamdi R, Hendry M, Kawai T, Kawamoto Y, Kondo H, Krayenhoff ES, Lee SH, Loridan T, Martilli A, Masson V, Miao S, Oleson K, Pigeon G, Porson A, Ryu YH, Salamanca F, Shashua-Bar L, Steeneveld GJ, Tombrou M, Voogt J, Young D, Zhang N (2010) The international urban energy balance models comparison project: first results from Phase 1. J Appl Meteorol Clim 49:1268–1292

Grimmond CSB, Blackett M, Best MJ, Baik JJ, Belcher SE, Beringer J, Bohnenstengel SI, Calmet I, Chen F, Coutts A, Dandou A, Fortuniak K, Gouvea ML, Hamdi R, Hendry M, Kanda M, Kawai T, Kawamoto Y, Kondo H, Krayenhoff ES, Lee SH, Loridan T, Martilli A, Masson V, Miao S, Oleson K, Ooka R, Pigeon G, Porson A, Ryu YH, Salamanca F, Steeneveld GJ, Tombrou M, Voogt JA, Young DT, Zhang N (2011) Initial results from Phase 2 of the international urban energy balance model comparison. Int J Climatol 31:244–272

Hagishima A, Narita KI, Tanimoto J (2007) Field experiment on transpiration from isolated urban plants. Hydrol Process 21:1217–1222

Johnson TD, Belitz K (2012) A remote sensing approach for estimating the location and rate of urban irrigation in semi-arid climates. J Hydrol 414:86–98

Kusaka H, Kondo H, Kikegawa Y, Kimura F (2001) A simple single-layer urban canopy model for atmospheric models: comparison with multi-layer and slab models. Boundary-Layer Meteorol 101:329–358
Kusaka H, Chen F, Tewari M, Dudhia J, Gill DO, Duda MG, Wang W, Miya Y (2012a) Numerical simulation of Urban Heat Island effect by the WRF Model with 4-km grid increment: an inter-comparison study between the urban canopy model and slab model. J Meteorol Soc Jpn 90B:33–45
Kusaka H, Hara M, Takane Y (2012b) Urban climate projection by the WRF model at 3-km horizontal grid increment: dynamical downscaling and predicting heat stress in the 2070's August for Tokyo, Osaka, and Nagoya metropolises. J Meteorol Soc Jpn 90B:47–63
Lantz N, Wang J (2010) Land cover information extraction using high resolution satellite data in Montreal. EPiCC Technical Report No. 5, 28 pp. http://www.epicc.ca/media-centre/presentations#TechDocs
Lee SH, Park SU (2008) A vegetated urban canopy model for meteorological and environmental modelling. Boundary-Layer Meteorol 126:73–102
Lemonsu A, Belair S, Mailhot J, Leroyer S (2010) Evaluation of the town energy balance model in cold and snowy conditions during the Montreal urban snow experiment 2005. J Appl Meteorol Clim 49:346–362
Loridan T, Grimmond CSB, Grossman-Clarke S, Chen F, Tewari M, Manning K, Martilli A, Kusaka H, Best M (2010) Trade-offs and responsiveness of the single-layer urban canopy parametrization in WRF: an offline evaluation using the MOSCEM optimization algorithm and field observations. Q J R Meteorol Soc 136:997–1019
Martilli A, Clappier A, Rotach MW (2002) An urban surface exchange parameterisation for mesoscale models. Boundary-Layer Meteorol 104:261–304
Masson V (2000) A physically-based scheme for the urban energy budget in atmospheric models. Boundary-Layer Meteorol 94:357–397
Mayer PW, Deoreo WBE (1999) Residential end uses of water. American Water Works Association, Denver, 310 pp
Miao S, Chen F (2014) Enhanced modeling of latent heat flux from urban surfaces in the Noah/single-layer urban canopy coupled model. Sci China Earth Sci 57:2408–2416
Miao S, Dou J, Chen F, Fan S (2012) Analysis of observations on the urban surface energy balance in Beijing. Sci China Earth Sci 55:1881–1890
Moriwaki R, Kanda M, Senoo H, Hagishima A, Kinouchi T (2008) Anthropogenic water vapor emissions in Tokyo. Water Resour Res 44:W11424
Myint SW, Gober P, Brazel A, Grossman-Clarke S, Weng QH (2011) Per-pixel vs. object-based classification of urban land cover extraction using high spatial resolution imagery. Remote Sens Environ 115:1145–1161
Oke TR (1979) Advectively-assisted evapotranspiration from irrigated urban vegetation. Boundary-Layer Meteorol 17:167–173
Oke TR (1988) The urban energy balance. Prog Phys Geog 12:471–508
Ramamurthy P, Bou-Zeid E (2014) Contribution of impervious surfaces to urban evaporation. Water Resour Res 50:2889–2902
Sailor DJ, Hart M (2006) An anthropogenic heating database for major US cities. In: Sixth symposium on the urban environment, Atlanta, Georgia, 28 January–3 February 2006
Sailor DJ, Lu L (2004) A top-down methodology for developing diurnal and seasonal anthropogenic heating profiles for urban areas. Atmos Environ 38:2737–2748
Sailor DJ, Brooks A, Hart M, Heiple S (2007) A bottom-up approach for estimating latent and sensible heat emissions from anthropogenic sources. In: Seventh symposium on the urban environment, San Diego, California, 10–13 September 2007
Salamanca F, Krpo A, Martilli A, Clappier A (2010) A new building energy model coupled with an urban canopy parameterization for urban climate simulations-part I. formulation, verification, and sensitivity analysis of the model. Theor Appl Climatol 99:331–344
Salamanca F, Martilli A, Tewari M, Chen F (2011) A study of the urban boundary layer using different urban parameterizations and high-resolution urban canopy parameters with WRF. J Appl Meteorol Clim 50:1107–1128
Santamouris M (2014) Cooling the cities—a review of reflective and green roof mitigation technologies to fight heat island and improve comfort in urban environment. Sol Energy 103:682–703
Senay GB, Budde M, Verdin JP, Melesse AM (2007) A coupled remote sensing and simplified surface energy balance approach to estimate actual evapotranspiration from irrigated fields. Sensors 7:979–1000
Song J, Wang ZH (2014) Interfacing the urban land-atmosphere system through coupled urban canopy and atmospheric models. Boundary-Layer Meteorol (in press). doi:10.1007/s10546-014-9980-9
Sun T, Bou-Zeid E, Wang ZH, Zerba E, Ni GH (2013) Hydrological determinants of green roof performance via a vertically-resolved model for heat and water transport. Build Environ 60:211–224
Tooke TR, Coops NC, Goodwin NR, Voogt JA (2009) Extracting urban vegetation characteristics using spectral mixture analysis and decision tree classifications. Remote Sens Environ 113:398–407

United Nations (2012) World urbanization prospects: the 2011 revision. The United Nations' Department of Economic and Social Affairs—Population Division, New York, 50 pp

van der Laan M, Tooke TR, Christen A, Coops N, Heyman E, Olchovski I (2011), Statistics on the built infrastructure at the Vancouver EPiCC experimental sites. EPiCC Technical Report No. 4, 30 pp. http://www.epicc.ca/media-centre/presentations/#TechDocs

Wang ZH (2014a) Monte Carlo simulations of radiative heat exchange in a street canyon with trees. Sol Energy 110:704–713

Wang ZH (2014b) A new perspective of urban-rural differences: the impact of soil water advection. Urban Clim 10:19–34

Wang ZH, Bou-Zeid E, Smith JA (2011a) A spatially-analytical scheme for surface temperatures and conductive heat fluxes in urban canopy models. Boundary-Layer Meteorol 138:171–193

Wang ZH, Bou-Zeid E, Au SK, Smith JA (2011b) Analyzing the sensitivity of WRF's single-layer urban canopy model to parameter uncertainty using advanced Monte Carlo simulation. J Appl Meteorol Clim 50:1795–1814

Wang ZH, Bou-Zeid E, Smith JA (2013) A coupled energy transport and hydrological model for urban canopies evaluated using a wireless sensor network. Q J R Meteorol Soc 139:1643–1657

Wang ZX, Jiang YH, Li J, Liu WD, Wang Q (2009) On the measurement of urban boundary layer radiation of the meteorological tower in Beijing (in Chinese). Plateau Meteorol 28:20–27

Yang J, Wang ZH (2014) Parameterization and sensitivity of urban hydrological models: application to green roof systems. Build Environ 75:250–263

Yang J, Wang ZH, Lee TW (2013) Relative efficiency of surface energy partitioning over different land covers. Brit J Environ Clim Change 3:86–102

Zhang CL, Chen F, Miao SG, Li QC, Xia XA, Xuan CY (2009) Impacts of urban expansion and future green planting on summer precipitation in the Beijing metropolitan area. J Geophys Res Atmos 114:D02116